

Tumor-targeting engineered probiotic *Escherichia coli* Nissle 1917 inhibits colorectal tumorigenesis and modulates gut microbiota homeostasis in mice

Haibo Tang^a, Tuoyu Zhou^a, Weilin Jin^c, Simin Zong^a, Tursunay Mamtimin^a, El-Sayed Salama^d, Byong-Hun Jeon^e, Pu Liu^a, Huawen Han^{a,b,*}, Xiangkai Li^{a,**}

^a Ministry of Education Key Laboratory of Cell Activities and Stress Adaptations, School of Life Science, Lanzhou University, Lanzhou, China

^b State Key Laboratory of Grassland Agro-ecosystems, Center for Grassland Microbiome, Lanzhou University, Lanzhou, China

^c Institute of Cancer Neuroscience, Medical Frontier Innovation Research Center, The First Hospital of Lanzhou University, The First Clinical Medical College of Lanzhou University, Lanzhou, China

^d Department of Occupational and Environmental Health, School of Public Health, Lanzhou University, Lanzhou, China

^e Department of Earth Resources and Environmental Engineering, Hanyang University, Seoul, Republic of Korea

ARTICLE INFO

Keywords:

Engineered probiotic
Escherichia coli Nissle 1917
AOM/DSS model
Tumor-targeting treatment
Gut microbiota

ABSTRACT

Aims: Preliminary studies have identified the use of probiotics as a potential treatment strategy against colorectal cancer (CRC). However, natural probiotics lack direct tumor-targeting and tumor-killing activity in the intestine. This study aimed to construct a tumor-targeting engineered probiotic to combat CRC.

Main methods: Standard adhesion assay was performed to analyze the adherence ability of tumor-binding protein HlpA to CT26 cells. CCK-8 assay, Hoechst 33258 staining and flow cytometry analysis were used for examining cytotoxicity of tumoricidal protein azurin toward CT26 cells. An engineered probiotic Ep-AH harboring *azurin* and *hlpA* genes was developed using *Escherichia coli* Nissle 1917 (EcN) chassis. Antitumor effects of Ep-AH were evaluated in the azoxymethane (AOM) and dextran sodium sulfate salt (DSS)-induced CRC mice. Moreover, analysis of gut microbiota was conducted via fecal 16S rRNA gene sequencing and shotgun metagenomic sequencing.

Key findings: Azurin caused a dose-dependent increase of apoptosis in CT26 cells. Ep-AH treatment reversed weight loss ($p < 0.001$), fecal occult blood ($p < 0.01$), and shortening of colon length ($p < 0.001$) than model group, as well as reducing tumorigenesis by 36 % ($p < 0.001$). Both Ep-H and Ep-A (EcN expressing HlpA or azurin) were less effective than Ep-AH. Furthermore, Ep-AH enriched the members of beneficial bacteria (e.g., *Blautia* and *Bifidobacterium*) and reversed abnormal changes of genes associated with several metabolic pathways (e.g., lipopolysaccharide biosynthesis).

Significance: These results demonstrated that Ep-AH had excellent therapeutic benefits on cancer remission and gut microbiota modulation. Our study provides an effective strategy for anti-CRC treatment.

1. Introduction

Colorectal cancer (CRC) was estimated to have 1.9 million new cases and cause 0.935 million deaths globally in 2020, rendering it the third most common cancer and the second leading cause of cancer-related death worldwide [1]. Conventional therapeutic regimes, such as surgery, chemotherapy, and radiotherapy, can provide significant benefits for patients in clinical practice. However, the choices of these treatments generally require consideration of tumor-related characteristics and

patient-related factors [2,3]. Thus, it is crucial to develop a novel and safe biological therapy.

Some studies showed gut microbiota is closely associated with CRC pathogenesis [4–6]. However, the major bacterial species that influence the development of CRC have not been thoroughly investigated. The intestines of CRC patients mainly enriched several bacterial species, including *Fusobacterium nucleatum*, enterotoxigenic *Bacteroides fragilis*, and pks⁺ *Escherichia coli* [4]. These strains promoted carcinogenesis by stimulating CRC cell proliferation [7,8]. In contrast, some probiotics,

* Correspondence to: H. Han, State Key Laboratory of Grassland Agro-ecosystems, Center for Grassland Microbiome, Lanzhou University, Lanzhou, China.

** Correspondence to: X. Li, Ministry of Education Key Laboratory of Cell Activities and Stress Adaptations, School of Life Science, Lanzhou University, Lanzhou, China.

E-mail addresses: hanhuawen@lzu.edu.cn (H. Han), xkli@lzu.edu.cn (X. Li).

<https://doi.org/10.1016/j.lfs.2023.121709>

Received 22 February 2023; Received in revised form 14 April 2023; Accepted 17 April 2023

Available online 24 April 2023

0024-3205/© 2023 Elsevier Inc. All rights reserved.

such as *Bifidobacterium animalis* and *Streptococcus thermophilus*, were decreased in CRC patients [9], and replenishing these probiotics may provide health benefits for the host. Based on the “gut remediation” concept, our previous study revealed that the probiotic *Limosilactobacillus fermentum* GR-3 could degrade and promote excretion of uric acid to ameliorate human hyperuricemia [10]. Moreover, as CRC originates in the intestine, we propose that whether this concept is feasible for treating CRC.

Probiotic-mediated CRC therapy has gained great attention owing to its excellent characteristic in gut microbiota regulation, which can be considered as a novel strategy to prevent and treat CRC [11]. Several reports showed that probiotics exhibited promising anti-CRC activities via correcting microbiota composition and modulating immune responses [12,13]. However, natural probiotics lack direct tumor-killing activity in the intestine [14,15]. Engineered probiotics contribute to addressing these issues via the delivery of various therapeutic payloads, such as cytotoxic proteins and angiogenesis modulation proteins [16], but they show poor performance in tumor targeting [14,17]. Therefore, it is essential to develop a comprehensive CRC treatment strategy that can target and kill CRC cells simultaneously.

Azurin has been considered as a promising tumoricidal protein [18,19], and a 28-amino-acid cell-penetrating peptide (p28) from azurin were applied in phase I clinical trials in patients with advanced solid tumors (including colon cancer) [20]. As an anchorless cell surface protein of *S. gallolyticus* [21], HlpA exhibited submicromolar affinity for CRC cell lines [17]. We hypothesized that the engineered probiotic harboring *hlpA* and *azurin* genes possessed an antitumor effect. In this study, an anti-CRC therapeutic bacteria Ep-AH was developed using *E. coli* Nissle 1917. We aimed to examine whether Ep-AH could protect colon against AOM/DSS, suppress tumorigenesis and modulate gut microbiota in the AOM/DSS mouse model.

2. Materials and methods

2.1. Engineered strains construction and cell cultivation

All genes' sequences, including *hlpA* [21], *azurin* [22], and two protein export tags (*pelB*, *inp*) [23,24], were synthesized by Qingke biotechnology (Nanjing, China). Expressions of these genes were achieved by sub-cloning into constitutive plasmid p20a (a modified pSB1A3 plasmid without mRFP sequence) using one-step Cloning Kit (Vazyme, China). The resultant recombinant plasmids were transformed into *E. coli* Nissle 1917 (EcN) for performance tests. The detailed information related to primers, recombinant plasmids, and engineered strains (Ep-A, Ep-H, and Ep-AH) were presented in Supplementary Table S1. All engineered strains were cultured in Luria Broth (LB) containing 50 mg/L ampicillin at 37 °C. Murine colon tumor CT26 cells (Procell, China) were cultured in Dulbecco's Modified Eagle Medium (DMEM, BasalMedia, China) containing 10 % fetal bovine serum and 1 % streptomycin/penicillin, and incubated at 37 °C under 5 % CO₂ atmosphere.

2.2. Growth curves and protein expression analysis of engineered bacteria

Fresh bacterial suspensions (2 mL) were inoculated in 200 mL of ampicillin-containing LB medium and cultured for 20 h. Samples were collected for OD₆₀₀ detection at 2-h intervals to evaluate whether the heterogeneous expression of HlpA and azurin influences the growth of EcN. In order to trace the expression locations of azurin and HlpA, the C-terminal 6 × His tag was introduced into strains Ep-A, Ep-H, and Ep-AH using the BKL Blunting Kit (Takara, China). The transformants were grown overnight in ampicillin-containing LB medium. Cultures were centrifuged (4500g, 10 min, 4 °C) to obtain supernatants and bacterial pellets. The supernatants of Ep-A and Ep-AH were filtered (0.22 μm pore filter) and concentrated by a centrifugal unit (Amicon® Ultra, 3 kDa, Millipore) [25]. Expression of azurin in the supernatants was verified with western blotting. Additionally, the bacterial pellets of Ep-H and Ep-

AH were resuspended in lysis buffer (20 mM Tris HCl, pH 8.0, 250 mM NaCl), followed by ultrasonication. The supernatants were collected by centrifugation (8000g, 15 min) for subcellular fractionation, as previously described [26]. The expressions of HlpA in respective components were detected using western blotting. Mouse anti-His-tag and HRP-labeled goat anti-mouse IgG served separately as primary and secondary antibodies.

2.3. Adhesion assays of Ep-H to CT26 cells

HlpA and red fluorescent protein (RFP) were coexpressed in strain Ep-H (RFP) for visualization of bacterial adherence efficiency, whereas Ep (RFP) that only expressed RFP was used as negative control. The adherence efficiency of Ep-H (RFP) to CT26 cells was measured using a standard adhesion assay [27]. Specifically, CT26 cells were seeded in 6-well cell culture plates at 2×10^5 cells/well and cultured for 24 h. The culture medium was substituted with new DMEM supplemented with 50 mg/L ampicillin. Ep-H (RFP) and Ep (RFP) with a bacterial density of 1×10^7 CFU were inoculated and co-cultured with CT26 cells for 2 h, respectively. Next, CT26 cells were washed twice using sterile PBS for eliminating the non-adherent bacteria, and stained with 4', 6-diamidino-2-phenylindole (DAPI) for visualization with the help of fluorescent microscope (Olympus IX71, Japan). Subsequently, Triton X-100 (at a 1 % volume-to-volume ratio) was added into culture wells, and incubating at 28 °C for 10 min for lysing CT26 cells. Serial 10-fold dilutions were prepared from the harvested cell lysates and spread on LB agar plates containing 50 mg/L ampicillin to obtain the CFU number of the adherence bacteria. This assay was repeated three times.

2.4. Cytotoxicity assays of azurin secreted by Ep-A toward CT26 cells

Azurin was collected and concentrated from the culture supernatant of Ep-A, as described previously. CT26 cells were seeded in 96-well plates (1×10^4 cells/well) and cultured for 24 h. Cells were treated with various concentrations of concentrated azurin secreted by Ep-A for 36 h, then 10 μL of CCK-8 reagent was added to each well for incubating at 37 °C for 1 h. OD_{450nm} of each well was measured by microplate reader (Multiskan GO, Thermo). Cell viability was calculated as described previously [28]. To investigate the effect of azurin secreted by Ep-A on cell apoptosis, after 36-h co-culture of CT26 cells and concentrated azurin, these cells were stained with Hoechst 33258 working fluid (KeyGEN BioTECH, China), according to manufacturer's instructions. Nuclear morphology was analyzed under a fluorescence microscope (Olympus IX71, Japan). Flow cytometry was used to further examine cell apoptosis. Various concentrations of concentrated azurin were incubated with CT26 cells for 36 h, respectively. Annexin-V FITC/PI staining was performed following kit instructions (Yeasen, China). Proportions of apoptotic cells were analyzed by the BD LSRFortessa™ cell analyzer and FlowJo V10 software.

2.5. Design of animal experiments

Seven-week-old female Balb/c mice were obtained from the animal center of Lanzhou University, and raised under standard temperature and humidity conditions, with a 12-h light/dark cycle. The animal experiment was approved by the Ethics Committee of the School of Life Sciences, Lanzhou University (Approval Number: EAF2022053).

A total of seventy-eight normal mice were used for animal experiments after five days of adaptive feeding in the laboratory. To investigate the function of Ep-H in vivo, eight mice were divided into two groups ($n = 4$ per group) and were separately treated with Ep and Ep-H. Another sixteen mice were used for the establishment of AOM/DSS-induced CRC model. They were also divided into two groups ($n = 8$ per group) and were treated with Ep and Ep-A, respectively. Subsequently, fifty-four mice were categorized into six groups for the functional evaluation of Ep-AH ($n = 9$ per group): (1) normal group (only

PBS treatment), (2) model group (only AOM/DSS treatment), (3) Ep group (AOM/DSS treatment and Ep), (4) Ep-A group (AOM/DSS treatment and Ep-A), (5) Ep-AH group (AOM/DSS treatment and Ep-AH), and (6) 5Fu group [AOM/DSS treatment and 5-fluorouracil (5Fu)]. To construct azoxymethane (AOM, MP Biomedicals, USA) and dextran sodium sulfate salt (DSS, Mw = 36–50 kDa, Yeasen, China)-induced colon carcinogenesis mouse model, mice were intraperitoneally injected with AOM (10 mg/kg body weight). After an interval of 5 days with normal feeding, the mice were treated with DSS-containing drinking water (at a 2.5 % weight-to-volume ratio) for 5 days, followed by regular drinking water for the next 16 days. The administration of DSS was repeated three times during the 63-day experimental period. The three strains (Ep, Ep-A, Ep-AH) were separately administered to the mice via oral gavage, with a bacterial density of 1×10^8 CFU after the initiation of DSS administration. The supplementations of strains were maintained three times per week. Meanwhile, 5Fu was fed to AOM/DSS mice twice per week via intraperitoneal injection (25 mg/kg body weight) at the beginning of DSS administration to serve as positive controls. Mouse body weights were measured weekly. The occult blood in the stool was determined at different intervals (2, 3, and 7 days). Bleeding analysis was performed as follows: gross bleeding and bleeding around the anus (scored 4), a positive hemocult result (scored 2), and no blood in the hemocult test (scored 0). After 63 days, all mice were sacrificed via CO₂ asphyxiation and subsequent cervical dislocation, and their colons were collected. Partial samples were used for detecting colon length, quantifying tumor numbers and being fixed in 4 % paraformaldehyde. The remaining samples were snap-frozen at -80°C for subsequent analyses.

2.6. Quantification of the distribution of Ep-H in the colon tissue

The AOM/DSS and normal mice were treated with Ep and Ep-H to explore the adhesion ability of Ep-H to different colonic segments. After a 63-day experiment, various colon segments (including approximately 1 cm of proximal, middle, and distal colonic tissues) were collected and washed with sterile 0.9 % NaCl solution immediately. These segments were longitudinally opened and scraped to obtain mucosal samples. The total bacterial DNA from mucosal samples was extracted by a Stool DNA Kit (Tiangen, China). Absolute quantification of Ep, Ep-H, and total 16S rDNA was performed via a quantitative PCR assay, as described previously [29]. The relative abundances of Ep and Ep-H in different colon segments were presented as the ratio of the absolute values of Ep and Ep-H to the total 16S rDNA. The specific primers for EcN and total bacteria were listed in Supplementary Table S2.

2.7. Immunohistochemical staining analysis

Paraffin-embedded tissue slides were processed for deparaffinization, rehydration and antigen retrieval. Slides were immersed in 3 % H₂O₂ solution to quench endogenous peroxidase prior to blocking with normal goat serum. Slides were incubated overnight at 4°C with the primary antibodies Bax and Bcl-2 (1:100, Bioss, China), followed by the biotinylated goat anti-rabbit secondary antibody (ZSGB-BIO, China). Fresh 3,3'-diaminobenzidine solution was dropped onto slides for staining. Hematoxylin was used for counterstaining to visualize nuclei. A brownish-yellow color indicates a positive result.

2.8. Total RNA extraction and qRT-PCR analysis

The total RNA from CT26 cells and distal colon tissues was extracted using RNAiso plus reagent (TaKaRa) based on manufacturer instructions, and quantified by NanoDrop 2000 spectrophotometer (Thermo Scientific). The obtained RNA was reverse-transcribed into cDNA with a Reverse Transcription Kit (TaKaRa, RR047A). qRT-PCR was conducted using TB Green (TaKaRa, RR820A) with the ABI QuantStudio 5 System to examine the expressions of the *p53*, *p21*, *Bax*, and *Bcl-2* genes. Relative genes expressions were analyzed with the

$2^{-\Delta\Delta\text{Ct}}$ calculation method using internal control GAPDH for normalization. All tests were repeated in triplicate. Detailed information of primers used are presented in Supplementary Table S2.

2.9. Fecal bacterial 16S rRNA gene sequencing analysis

Total stool DNA extractions were performed by a QIAamp DNA Stool Mini Kit (Qiagen). DNA quality was examined using 1.0 % agarose gel electrophoresis. The V3-V4 region of the 16S rRNA gene was amplified with the primer pairs 338F and 806R [30]. Amplified products were measured with the Quant-iT dsDNA Kit (Invitrogen). High-throughput sequencing was conducted based on the Illumina MiSeq platform. Subsequently, bioinformatics processing was performed using the QIIME2 platform (version 2019.04, <https://qiime2.org/>). Chao1 and Shannon indices were used for the α -diversity evaluation of gut microbiota. β -diversity was evaluated by principal coordinate analysis (PCoA) based on Bray-Curtis distance. Composition of taxa at phylum and genus levels was analyzed. The relationship between gut microbiota and the expressions of apoptosis-related genes was identified via spearman correlation analysis.

2.10. Metagenomic sequencing, assembly, and functional annotations of fecal samples

Total stool DNA extraction and quality examination were conducted, as described previously. DNA sample was mechanically sheared to approximately 400 bp using a Covaris M220 ultrasonicator. The resulting DNA fragments were used for the construction of the paired-end libraries with the NEXTFLEX™ Rapid DNA-Seq Kit (Bioo Scientific); 2×150 -bp paired-end metagenomes sequencing was performed through the Illumina NovaSeq platform.

Raw reads were processed to generate clean reads with high quality using the Fastp v0.20.0 software [31]. Any reads with high similarity to mouse host genome were removed for generating the high-quality reads using the BWA v0.7.17 software [32]. Metagenomics data were assembled using MEGAHIT v1.1.2 [33]. The obtained contigs with ≥ 300 bp in length were retained. The ORF prediction was performed using a MetaGene [34], and gene sequences with a length of ≥ 100 bp were translated into amino acid sequences. Subsequently, the predicted gene sequences were clustered for the construction of the non-redundant genes set based on ≥ 90 % identity and read coverage by CD-HIT v4.6.1 [35]. High-quality reads were aligned to non-redundant gene catalogs to determine gene abundance with ≥ 95 % identity by SOAP-aligner [36]. The gene sets were annotated using Diamond according to the NR and KEGG databases with the parameters “blastp; E-value $\leq 1e-5$ ” [37]. The differences of metabolic function in the KEGG level 3 pathway were analyzed using STAMP software.

2.11. Statistical analysis

All data were presented as the mean \pm SD, and were visualized by GraphPad Prism 8.3. As for the significant differences analysis, unpaired two-tailed student's *t*-test was used for the comparison of two groups, and an analysis of variance (ANOVA) followed by Tukey's post-test was used for multiple comparisons. $p < 0.05$ represents a significant difference. NS ($p > 0.05$) indicates no significant difference.

3. Results

3.1. Enhanced adhesion of Ep-H to CT26 cells in vitro

The fusion expressions of RFP and INP-HlpA were induced with constitutive promoter J23114 in Ep-H (RFP) strain, whereas the expression of RFP was manipulated by J23100 promoter in Ep (RFP) (Fig. 1a). Western blotting analysis demonstrated that the INP-HlpA fusion protein was successfully anchored to the surface of Ep-H

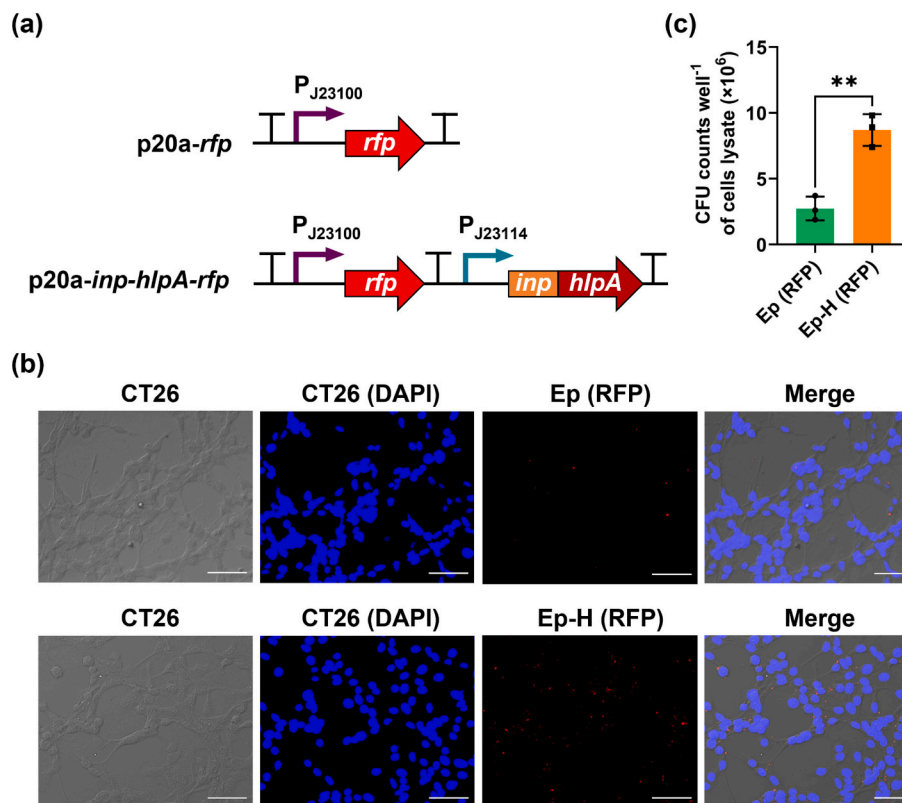


Fig. 1. The binding of Ep-H to CT26 cells. (a) A schematic feature of the construction of HlpA expression system. (b) Fluorescence microscopic image of Ep-H adhering to CT26 cells. DAPI was used for the cell nucleus staining (blue). Scale bar: 20 μ m. (c) Quantitative analysis of the adherent bacteria with the dilution method of plate counting. ($n = 3$, $*p < 0.05$).

(Fig. S1a). Fluorescence microscopic images revealed that larger amounts of Ep-H were bound to CT26 cells compared with the control Ep (Fig. 1b). Furthermore, spread plate assay showed that the number of CFU of adherent bacteria was significantly higher in the Ep-H group ($8.7 \pm 1.2 \times 10^6$ CFUs/well) than that observed in the Ep group ($2.7 \pm 0.9 \times 10^6$ CFUs/well) (Fig. 1c). These results indicated that cell surface-displayed HlpA enhanced the adherence of EcN to CT26 cells.

3.2. Cytotoxicity associated with azurin secreted by Ep-A in vitro

An azurin secretion expression system was constructed with the pelB secretion tag for directing protein secretion under the control of the J23100 promoter (Fig. 2a). Western blotting analysis demonstrated the expression of azurin in the culture supernatant of Ep-A (Fig. S1a). Under the condition of co-culture of CT26 cells and azurin-containing bacterial supernatants (ranging from 100 to 800 mg/L), morphological analysis revealed that cells lost adherent phenotype and exhibited an irregular shape (Fig. S2). For CCK-8 assays, azurin-containing bacterial supernatant showed a dose-dependent suppression on the proliferation of CT26 cells (Fig. 2b). Furthermore, Hoechst 33258 staining of treated CT26 cells revealed obvious characteristics of apoptosis, including karyopyknosis and nuclear hyperchromatism (Fig. 2c). Flow cytometry assays indicated that the rate of apoptotic cells increased by 12.1 %–62.5 % compared with the control (4.65 %) when the concentration of azurin-containing bacterial supernatant exceeded 100 mg/L (Fig. 2d, e). qRT-PCR further showed that the exposure of CT26 cells to azurin significantly enhanced the expressions of the proapoptotic genes *p53*, *p21*, and *Bax* in a dose-dependent manner and decreased the expression of the antiapoptotic gene *Bcl-2* (Fig. 2f). Collectively, these data confirmed that azurin could induce the apoptosis of CT26 cells in a dose-dependent manner.

3.3. HlpA mediated the specific binding of EcN to cancerous colon tissue in AOM/DSS mice

To investigate the quantification and distribution of engineered probiotics in different colonic segments, Ep and Ep-H were administered to normal and AOM/DSS mice, respectively (Fig. S3). Tumors mainly occurred in the distal colon tissue of AOM/DSS mice (Fig. 3a). The relative abundance of Ep-H was higher than that of Ep in the distal colon of AOM/DSS mice (Fig. 3b), whereas the distribution of Ep and Ep-H in all colon segments of normal mice showed negligible difference (Fig. 3c). These data indicated that HlpA mediated the specific binding of EcN to cancerous sites rather than healthy colon tissue (Fig. 3d). Although Ep-H exhibited enhanced adherence to the distal colon of AOM/DSS mice, the body weight, bleeding core, and tumorigenesis showed no significant difference between the Ep and Ep-H groups (Fig. S4). Thus, we speculated that the coexpression of tumor-targeting proteins and tumoricidal proteins may have excellent performance in CRC treatment.

3.4. Engineered probiotic Ep-AH attenuated the development of AOM/DSS-induced CRC

To further improve the treatment effect of EcN on CRC, an engineered probiotic Ep-AH harboring *azurin* and *hlpA* genes was constructed to evaluate its antitumor potential in AOM/DSS mice. Ep and Ep-A were used as negative controls, and the 5Fu group was chosen as positive control (Fig. 4a). The growth ability of several engineered probiotics was similar to that of EcN, indicating that the introduction of HlpA and azurin had no impact on bacterial cell growth (Fig. S5). AOM/DSS treatment severely decreased the body weight of mice, whereas both Ep-AH and 5Fu administration alleviated its weight loss (Fig. 4b). Moreover, Ep-AH and 5Fu group exhibited low bleeding score compared

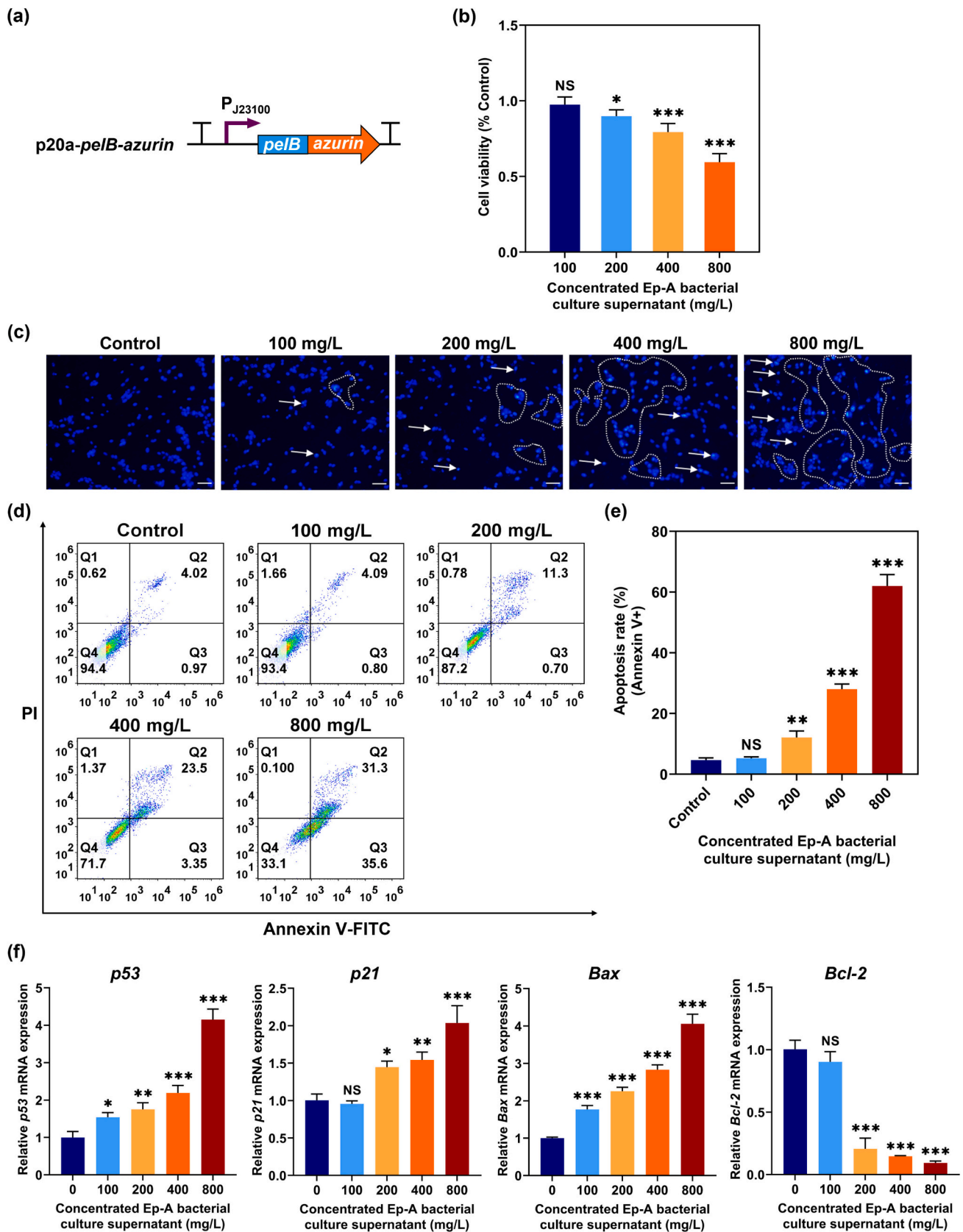


Fig. 2. Antitumor activity of azurin in the bacterial culture medium. (a) The schematic feature of the construct of azurin secretion expression system. (b) Viability of CT26 was assessed by CCK-8 assay ($n = 5$). (c) Effects of azurin on cell morphology. Scale bar: 200 μ m. (d) Apoptosis was evaluated by annexin V/PI double staining. (e) The quantitative analysis of the rate of apoptotic cells ($n = 3$). (f) The mRNA quantification of *p53*, *p21*, *Bax* and *Bcl-2* with qRT-PCR ($n = 3$). The mRNA level of these genes was normalized with that of the internal control GAPDH. Cells that were not treated with azurin-containing bacterial supernatant were considered as control. (* $p < 0.05$, ** $p < 0.01$, *** $p < 0.001$ vs. control; NS: no significant difference).

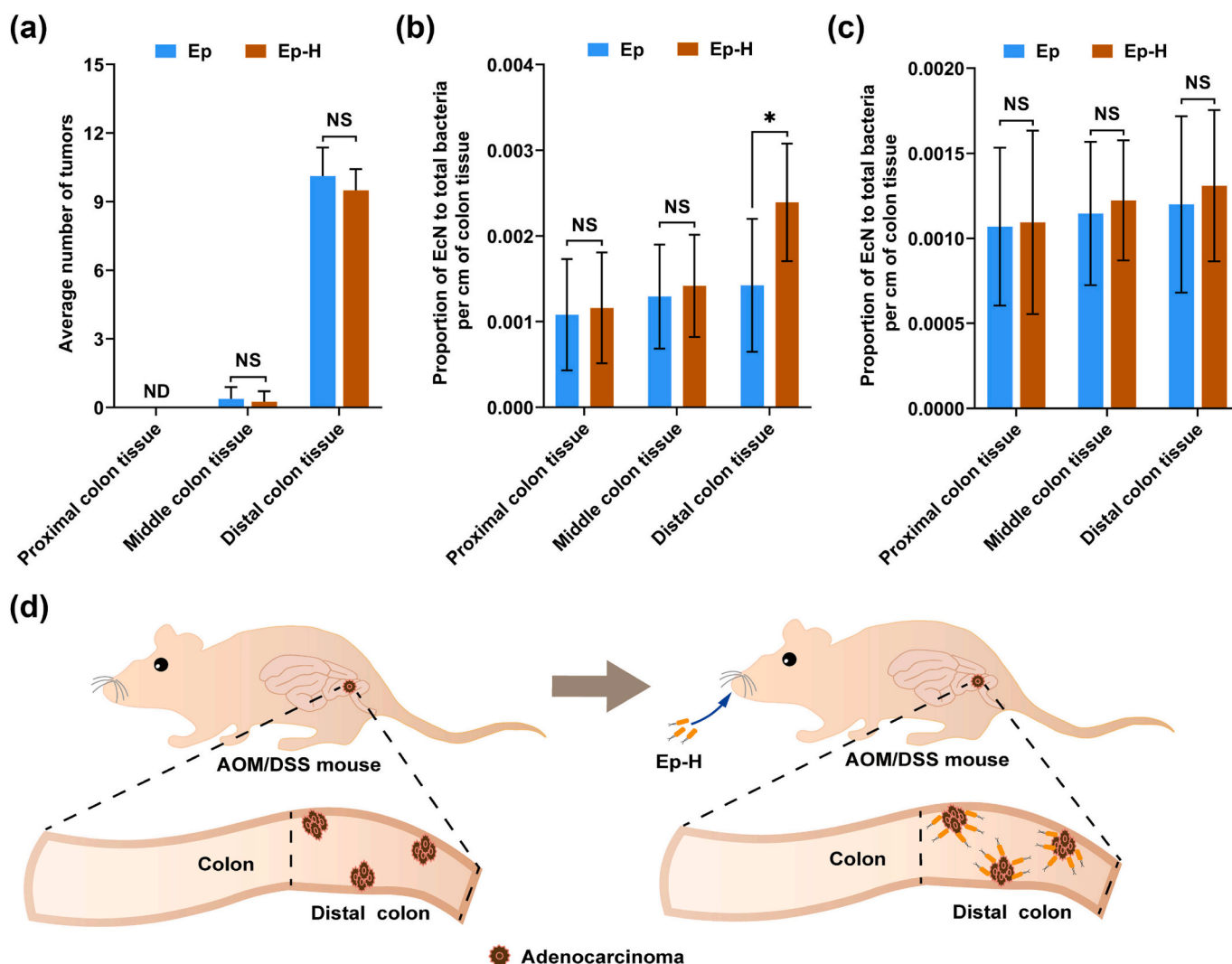


Fig. 3. Distribution of Ep-H in different colon segments in mice. (a) Average number of tumors from three different segments of the colon in AOM/DSS mice. The binding of bacteria to the proximal, middle, and distal colon segments was measured in both AOM/DSS mice (b) and normal mice (c) after 63 days. (d) The potential therapeutic mechanism of Ep-H in AOM/DSS mice. ($n = 8$ mice per group for (b), $n = 4$ mice per group for (c), $*p < 0.05$; ND: not detected; NS: no significant difference).

with model group, Ep and Ep-A ($p < 0.01$; Fig. 4c). Compared with the normal group, the colon length decreased after AOM/DSS treatment, but Ep-AH and 5Fu group suppressed AOM/DSS-induced shortening of the colon ($p < 0.001$; Fig. 4d, e). Model group exhibited a high tumor burden, whereas Ep-AH treatments decreased the number of tumors by 36 % (Fig. 4f). Notably, the tumor burden in the 5Fu group was the lowest among the AOM/DSS treatment groups (Fig. 4f).

3.5. Effects of Ep-AH on the expression of apoptosis-related factors in vivo

Given that azurin-mediated apoptosis of CT26 cells in vitro, we further investigated the possibility of Ep-AH regulating the expressions of proteins associated with apoptosis in vivo. qRT-PCR analysis revealed that supplementation of Ep-AH significantly enhanced the relative mRNA levels of *p53*, *p21*, and *Bax*, accompanied by decreasing the relative mRNA level of *Bcl-2* in the distal colon tissue compared with normal and model groups. In addition to *Bax*, the expressions of the other three apoptotic genes in the Ep-AH and 5Fu group showed insignificant difference (Fig. 5a). Furthermore, immunohistochemical staining confirmed that Ep-AH reversed the abnormal expression levels of the apoptotic factors *Bax* and *Bcl-2* in the model group (Fig. 5b). These findings suggested that Ep-AH could induce apoptosis in the colonic

carcinoma tissue by upregulating proapoptotic gene expression and downregulating antiapoptotic gene expression.

3.6. Ep-AH alleviated microbial dysbiosis in AOM/DSS mice

The gut microbiota analysis was used to further explore the potential mechanism of Ep-AH-mediated tumorigenesis amelioration in AOM/DSS mice. The Chao1 and Shannon indices of all groups showed no significant difference (Fig. 6a). PCoA analysis revealed that the normal and 5Fu groups shared distinct distributions with other groups. The community structures of the Ep-A and Ep-AH were significantly close, as well as the Ep and model group (Fig. 6b). At the phylum level, Bacteroidetes, Firmicutes, and Proteobacteria were the most dominant phyla of mouse gut microbiota (Fig. 6c). Firmicutes-to-Bacteroidetes ratio was significantly reduced in the model group compared with the normal group. Ep-AH administration reversed this phenomenon caused by AOM/DSS, whereas 5Fu group did not show this effect (Fig. S6a). At the genus level, AOM/DSS treatment caused an obvious decrease in number of beneficial *Lactobacillus* and *Bifidobacterium* and an increase in relative abundance of *Prevotella* compared with the normal group, whereas Ep-A and Ep-AH restored their relative abundances to the level of normal group (Fig. 6d-e, Fig. S6b). Additionally, the relative abundance of

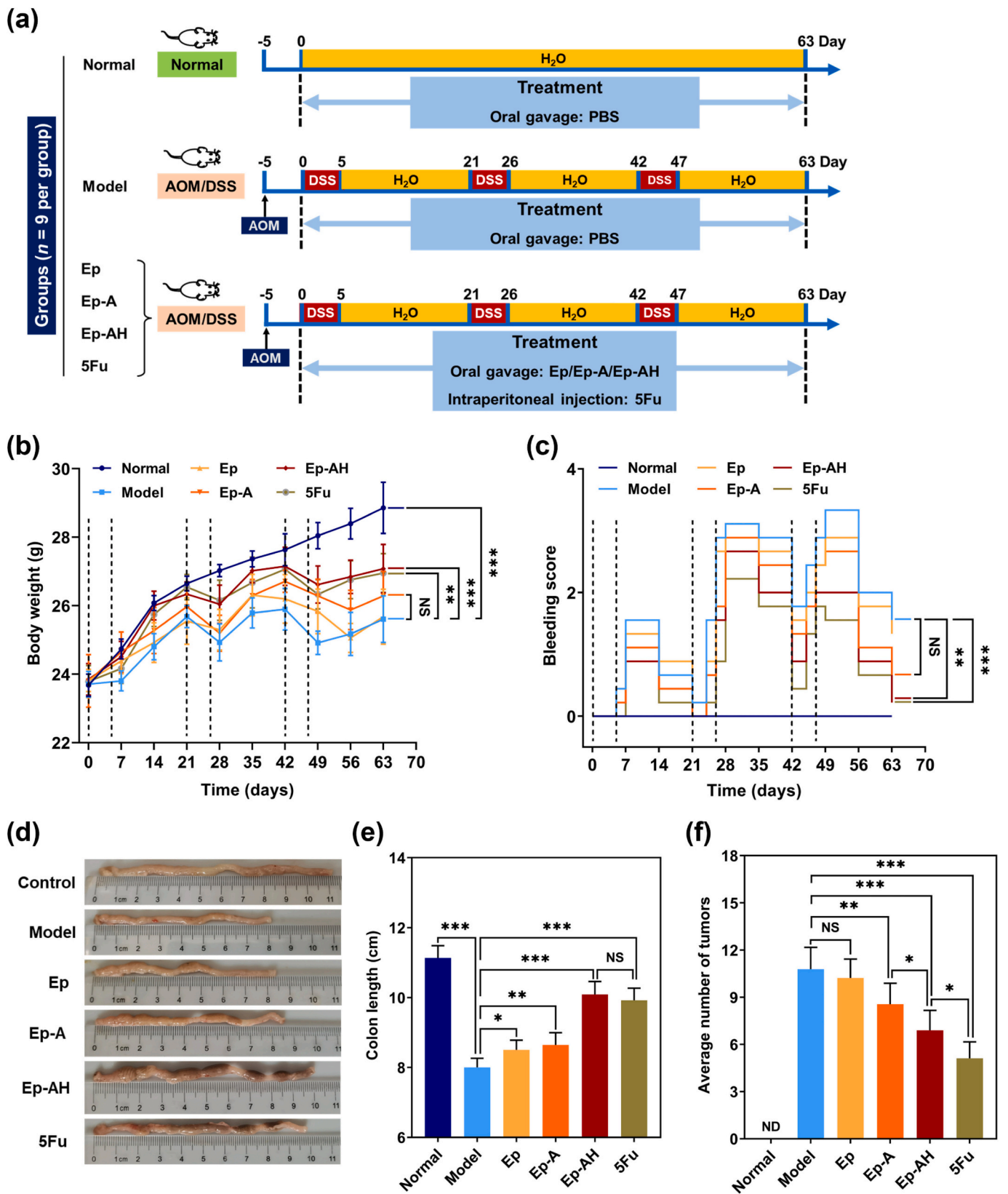


Fig. 4. Effects of Ep-AH on AOM/DSS mice. (a) An experimental schedule for the construction of the AOM/DSS model, grouping design and treatment protocols. (b) Body weight changes were recorded every 7 days ($n = 9$ mice per group). (c) Bleeding scores were assessed every 3, 2, or 7 days ($n = 9$ mice per group). (d) Representative images of colons of the groups ($n = 9$ mice per group). (e) Colon length and (f) average number of tumors ($n = 9$ mice per group). Dashed lines represent five days of DSS treatment. (* $p < 0.05$, ** $p < 0.01$, *** $p < 0.001$; ND: not detected; NS: no significant difference).

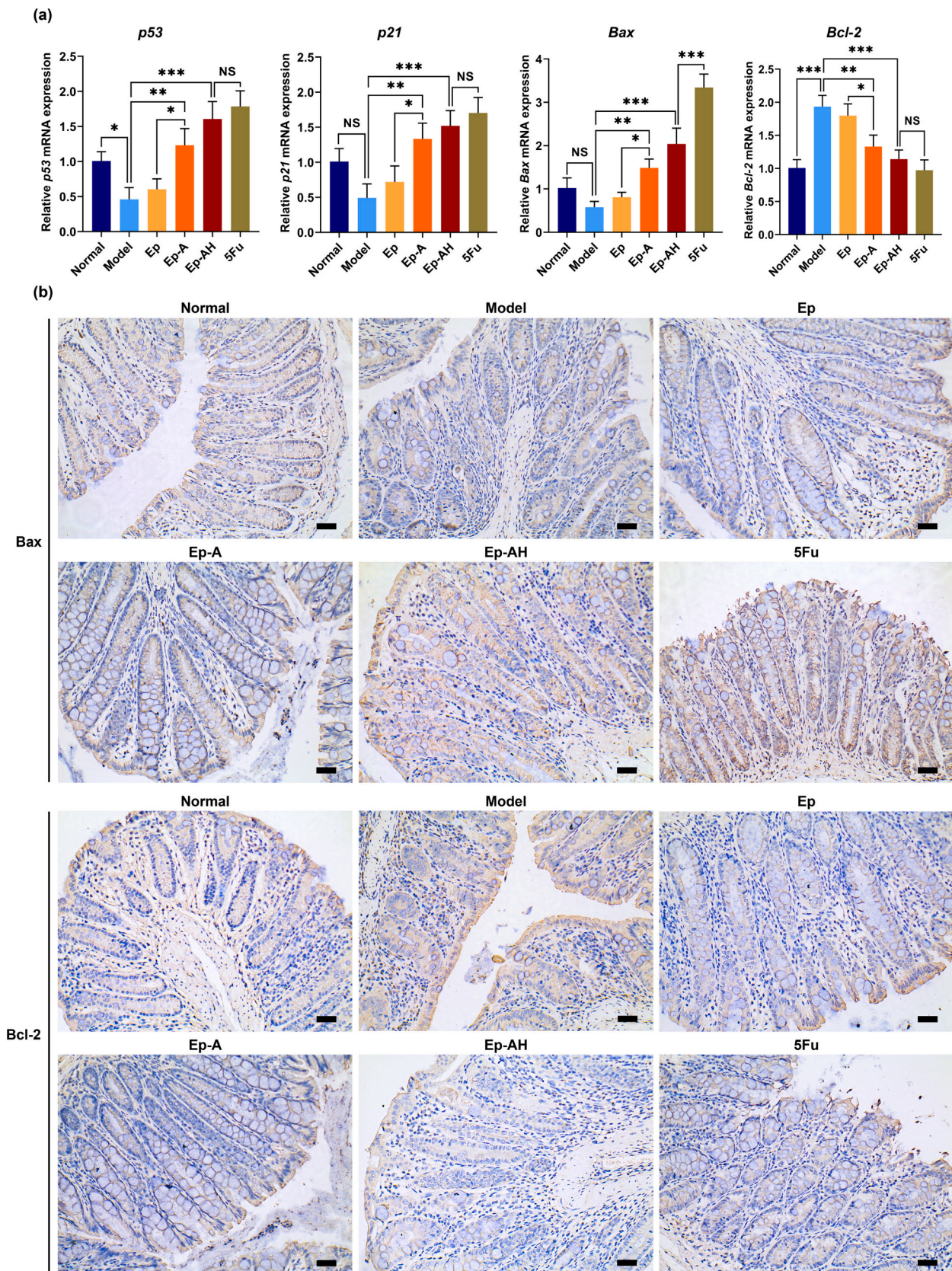


Fig. 5. Effects of Ep-AH on expression of apoptosis-related factors in distal colon tissues. (a) Relative gene expression differences of proapoptotic and antiapoptotic factors ($n = 3$). * $p < 0.05$, ** $p < 0.01$, *** $p < 0.001$; NS: no significant difference. (b) Immunohistochemical staining of Bax and Bcl-2. Scale bar: 40 μm .

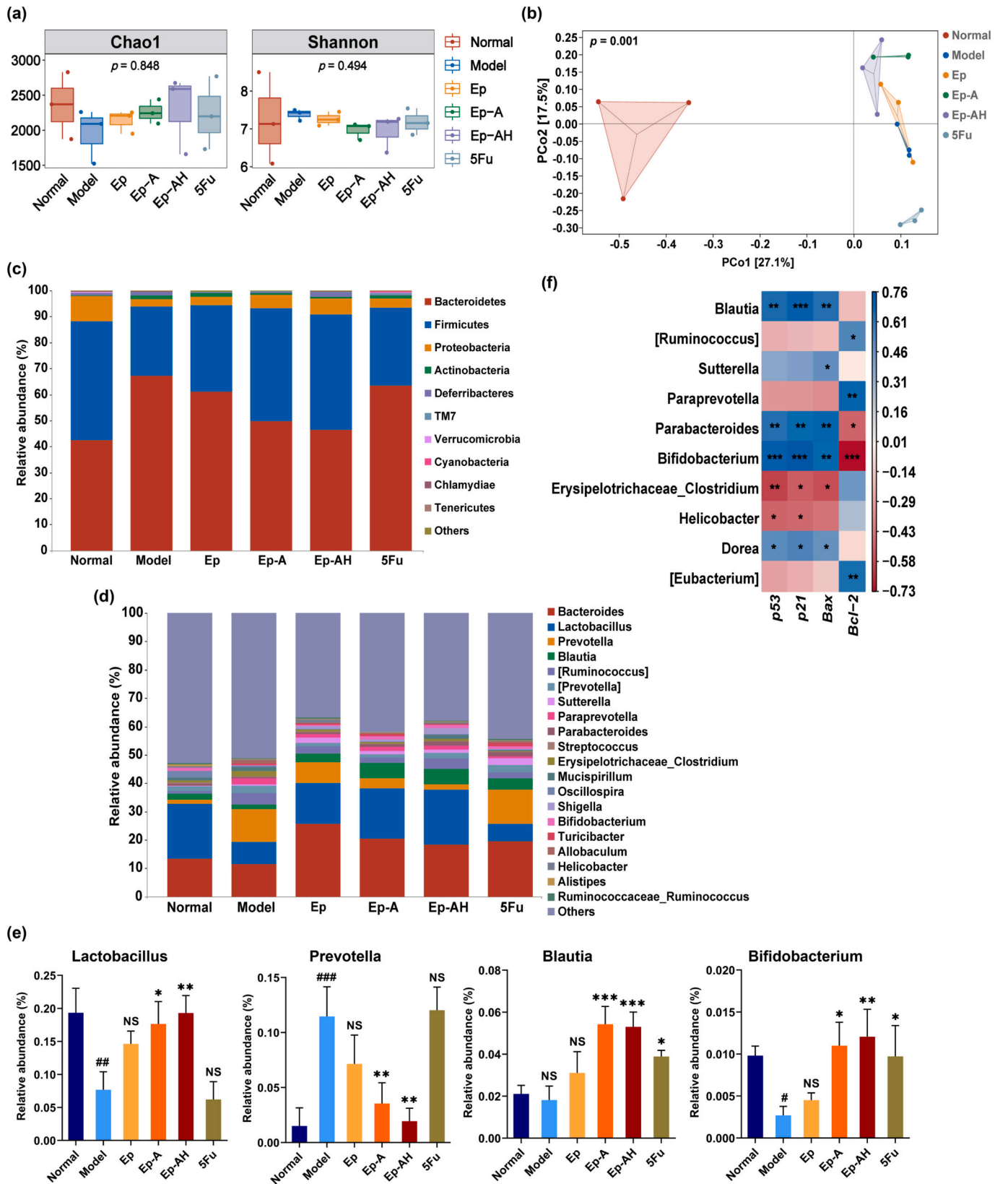


Fig. 6. Effects of Ep-AH on gut microbiome in AOM/DSS mice. (a) The α -diversity were assessed by Chao1, Shannon indices. (b) Principal coordinate analysis (PCoA) was visualized by Bray-Curtis distance. The difference test among the groups was performed using analysis of similarities. (c-d) Bacterial community composition analysis at phylum (c) and genus (d) levels. (e) Relative abundances of the representative bacteria at genus level. # $p < 0.05$, ## $p < 0.01$ vs. normal group; * $p < 0.05$, ** $p < 0.01$, *** $p < 0.001$ vs. model group; NS: no significant difference. (f) Correlation between gut microbiome and apoptosis-related factors was assessed with Spearman correlation analysis. Significant correlations were noted: * $p < 0.05$, ** $p < 0.01$, *** $p < 0.001$.

Blautia from Ep-A and Ep-AH was approximately 2.5-fold higher than that observed in the model and normal groups (Fig. 6d–e, Fig. S6b). The spearman correlation analysis between apoptosis-related genes in the colonic tissue and the microbial community found that *Bifidobacterium* and *Blautia* displayed positive correlations with *p53*, *p21*, and *Bax* levels and had negative correlations with *Bcl-2* levels. Similar phenomenon was also found in other genera, including *Sutterella* and *Dorea*. In contrast, *Paraprevotella*, *Erysipelotrichaceae_Clostridium*, and *Helicobacter* were negatively correlated with the *p53*, *p21*, and *Bax* indices, whereas the *Bcl-2* level was significantly correlated with *Paraprevotella* (Fig. 6f). Together, these findings suggested that Ep-AH relieved gut dysbiosis and restored its homeostasis in AOM/DSS mice.

3.7. Administration of Ep-AH restored the functional characteristics of the gut microbiome

To further assess whether Ep-AH administration altered the metabolic pathways of gut microbiome, a total of twelve fecal samples from normal, model, and Ep-AH groups were selected for metagenomic sequencing. The final gene catalog of 1,254,630 nonredundant genes was assembled, with an average length of 618.43 bp. Metagenome- and 16S amplicon-based profiles shared similar genus-level taxonomic abundances (Fig. S7). Among the 414 affiliated KEGG level 3 pathways, model group generated sixteen distinct pathways compared with normal group. Fifteen differential metabolic pathways were observed between normal group and Ep-AH, and five differential pathways were found between model and Ep-AH groups (Fig. S8). In contrast to other groups, the relative abundances of functional genes related to lipopolysaccharide biosynthesis were increased in the model group (Fig. 7a, c). However, Ep-AH decreased the amount of these functional genes to the level of the normal group (Fig. 7c). Furthermore, the high relative abundance of genes involved in ABC transporters from the model group was decreased by Ep-AH (Fig. 7d), as well as other functional genes of metabolic pathways, including aminoacyl-tRNA biosynthesis, homologous recombination, and pyrimidine metabolism (Fig. S9). Compared to the other two groups, the proportion of functional genes related to the biosynthesis of secondary metabolites significantly increased after Ep-AH administration (Fig. 7b, e). To further determine the species with differences in the contribution of the three identified metabolic functions, an association analysis between functional genes and species was performed (Fig. 7f). The relative contribution of *Alistipes* to the lipopolysaccharide biosynthesis was significantly higher in the model group ($2.73 \pm 0.45\%$) than that in the normal group ($0.87 \pm 0.46\%$) and Ep-AH ($1.49 \pm 0.50\%$). As for the ABC transporters, the relative contribution of *Prevotella* was $7.81 \pm 1.32\%$ in the model group, which was markedly increased in comparison to normal group ($1.24 \pm 0.60\%$) and Ep-AH ($5.28 \pm 1.17\%$). Additionally, the relative contributions of *Lactobacillus* and *Bifidobacterium* to the biosynthesis of secondary metabolites in the Ep-AH group were 3.3- and 10.0-fold higher than those in the normal group, and they were 3.9- and 3.0-fold higher than those in the model group, respectively. Collectively, these findings indicated that Ep-AH regulated and improved the metabolic functions of the gut microbiome.

4. Discussion

Novel neoadjuvant therapy (e.g., probiotic therapeutic) represents a promising approach for CRC owing to the close association between intestinal flora and CRC tumorigenesis. In this study, an engineered probiotic harboring *hlpA* and *azurin* genes were used for CRC treatment based on a “targeted killing” strategy. Adhesion assay observed a 3.18-fold increase in the adhesion of Ep-H to CT26 cells compared to Ep, which was similar with a previous study of EcN expressing INP-HlpA [17]. Common tumor-specific binding proteins have the ability to enhance the affinity of bacteria to tumor cells [17,38–40]. Among them, HlpA could bind to the cell surface of CRC cells by targeting the heparan

sulfate proteoglycan [17,41,42]. Azurin preferentially penetrates cancer cells and exert cytostatic without apparent toxicity to healthy cells [19,43]. Our results showed that azurin secreted by Ep-A showed a dose-dependent inhibitory effect on the proliferation of CT26 cells, which could be supported by another study reporting that the p28 peptide from azurin exerted cytostatic effects on HCT116 and HT29 CRC cells [22]. Furthermore, the proliferation suppression effect of azurin was associated with apoptosis (Fig. 2). Previous study found that Azurin induced apoptosis in U2OS cells by increasing the expressions of *p53* and *Bax* genes and decreasing *Bcl-2* gene expression [44]. Our observations shared similar findings in azurin-treated CT26 cells. Azurin exposure also resulted in the upregulation of *p21* gene, suggesting a potential cell cycle arrest effect of azurin.

The AOM/DSS-induced CRC murine model has been widely used to examine the effects of new drugs on CRC owing to its similar pattern of tumorigenesis and progression to human CRC [45]. In this study, tumors were primarily distributed in the distal colon of AOM/DSS mice, consistent with earlier studies [46,47]. Ep-H exhibited a higher affinity for tumor tissue in the distal colon than noncancerous tissue. Contrastly, the distributions of Ep-H and Ep were equivalent in all colon segments from normal mice. Similar findings were also observed in the study reported by Ho et al. [17]. Nonetheless, no positive correlation was observed between the high adhesion of Ep-H and its therapeutic effect. AOM/DSS treatment induced a series of abnormal symptoms in mice, such as body weight loss, high rectal bleeding, shortening of colon length, and adenoma initiation [17,48]. These symptoms could be effectively alleviated by Ep-AH treatment. The effects of Ep-AH were superior to that of Ep-A, indicating the greater therapeutic potential of difunctional engineered probiotic. As a first-line therapeutic drug for CRC [49], our study found that 5Fu and Ep-AH separately led to 53% and 36% reductions in tumor number. The treatment of 5Fu caused a 50% reduction in polyp number of AOM/DSS mice [50], and a 60–80% reduction in *Apc*^{min/+} mice [51]. Previous studies observed a significant weight loss under 5Fu administration in AOM/DSS mice [48,50], which contradicted the weight recovery reported in our study. The potential reason may be the difference in administration dosage. Administration of 20 mg/kg 5Fu showed no significant effect on body weight compared to model mice [52].

Apoptosis is of importance in modulating tumorigenesis [53]. Our observations found that AOM/DSS led to the upregulation expression of *Bcl-2*, and the downregulation of *p53*, *p21*, and *Bax* [54,55]. These changes were reversed by both Ep-A and Ep-AH, indicating that these strains accelerated the apoptosis of CRC cells via regulating the expressions of apoptosis-associated genes. As expected, Ep-A had a weaker effect than Ep-AH, implying that difunctional Ep-AH increased apoptosis in the colonic carcinoma tissue.

AOM/DSS is known to cause intestinal dysbacteriosis in mice [56,57]. Bacteroidetes was closely related to the promotion of tumorigenesis, whereas Firmicutes might constitute an effective treatment for inflammation and tumor of the colon [58]. The Ep-AH group exhibited a higher Firmicutes-to-Bacteroidetes ratio, which supported its beneficial effect on CRC treatment. Probiotics *Lactobacillus* and *Bifidobacterium* can offer protection against CRC [59], Ep-AH administration reversed the downward trend of these two bacteria caused by AOM/DSS, along with the enhanced relative abundance of *Blautia*. The high abundance of *Blautia* helps to maintain intestine homeostasis and suppresses inflammation by producing short chain fatty acids (SCFAs) [60]. After being treated with Ep-AH, the high abundance of *Prevotella* in the model and 5Fu groups could be decreased to the normal level, reflecting a mitigation effect of Ep-AH. Furthermore, spearman correlation analysis confirmed the benefits of *Bifidobacterium* and *Blautia* in regulating the apoptotic responses of CRC cells (Fig. 6f). Associated proapoptotic effects may be related to several active bacterial metabolites, such as bacteriocin and SCFAs [61,62]. Fecal metagenomic analysis indicated that Ep-AH administration reduced the number of genes related to LPS biosynthesis caused by AOM/DSS. Lipopolysaccharide (LPS) could

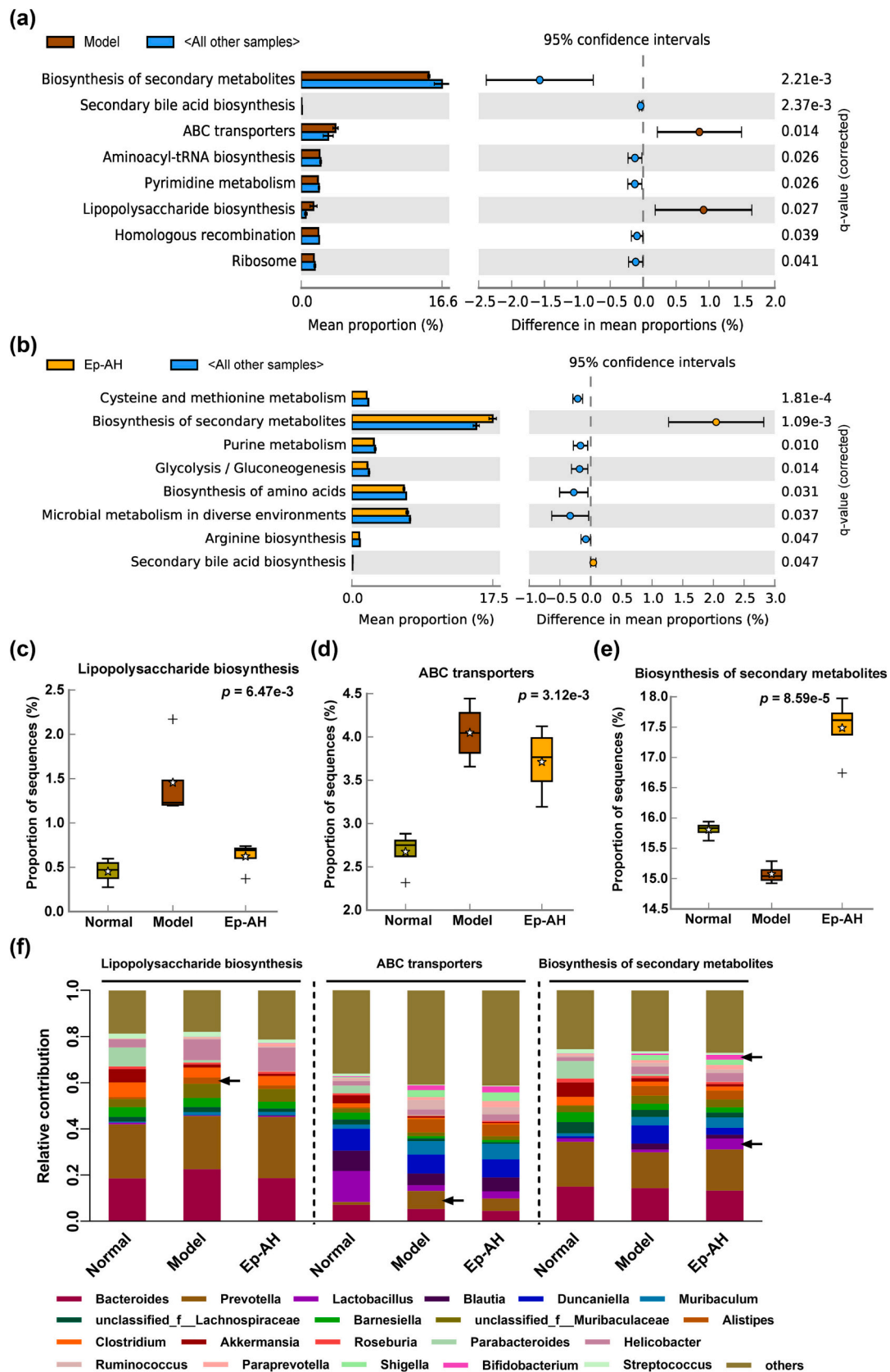


Fig. 7. Ep-AH treatment partially restored the functional characteristics of the gut microbiota. (a–b) Comparative analysis of the differences in metabolic pathways among the model group, Ep-AH group, and other groups. (c–e) The proportion of sequences (%) of the metabolic pathways with significant statistical difference in each group. (f) Relative contribution of different taxa at genus level to metabolic pathways of lipopolysaccharide biosynthesis, ABC transporters, and biosynthesis of secondary metabolites. Welch's *t*-test was used for comparative analysis between two groups. Kruskal–Wallis H test was used for comparative analysis among three groups. Multiple test correction was performed using Benjamin-Hochberg FDR ($p < 0.05$).

promote CRC cell proliferation via inducing toll-like receptor 4 signaling [63]. The Ep-AH group also increased the genes responsible for biosynthesis of secondary metabolites by 17.8 %. Several bacteria-derived metabolites have been shown to possess anti-CRC activities [64,65]. These results implied that Ep-AH had a protective effect against CRC development. Furthermore, beneficial bacteria (*Lactobacillus*, *Bifidobacterium*), and harmful bacteria (*Alistipes*) enhanced the biosynthesis of secondary metabolites and lipopolysaccharide, respectively. Of these, *Lactobacillus* and *Bifidobacterium* could generate beneficial SCFAs and secondary bile acids [65,66]. On the contrary, *Alistipes* was positively associated with LPS production and CRC carcinogenesis [57,67].

The use of radiation, chemotherapy, or combined chemoradiation maintained an unsatisfying pathological complete response rate of <15 % [68], and caused various side effects, such as gastrointestinal injury and neurotoxicity [69,70]. In contrast, probiotic-mediated CRC therapy can restore intestinal dysbacteriosis by modulating gut microbiota with minimal side effects [71]. More importantly, combination therapy of probiotics and conventional anticancer drugs has been proven to improve the efficiency of antitumor drugs and alleviate their side effects [72]. For example, *Bifidobacterium* supplementation relieved mucositis and gastrointestinal reactions during radiotherapy and chemotherapy [73]. Although substantial advances have been made in bacteria-mediated cancer therapy, some candidate natural probiotics for CRC therapy have unresolved issues, such as characterization and formulation during clinical trials [74]. In case of engineered bacteria, genetic stability and safety concerns also need to be carefully evaluated [14,75]. Nonetheless, we believe that bacteria-mediated cancer therapy still holds exceptional advantages and good prospects in the treatment of gastrointestinal tumors due to its direct interaction with gut microbes.

5. Conclusion

In this study, an engineered probiotic Ep-AH was constructed to express HlpA and azurin simultaneously based on a “targeted killing” strategy. HlpA binding assays and cytotoxicity tests confirmed the functions of these two genes. Importantly, Ep-AH exhibited excellent antitumor effects in AOM/DSS mice. Furthermore, Ep-AH with the probiotic characteristics of EcN chassis improved gut microbiota dysbiosis and abnormal metabolic functions. Therefore, our engineered probiotic Ep-AH can serve as a potential candidate in microbiome therapeutics for CRC. This study extends the application of tumor-targeting engineered probiotics in orthotopic CRC treatment and provides insights into the interaction of engineered commensal microbe with gut microbiota.

CRedit authorship contribution statement

Haibo Tang: Methodology, Investigation, Writing – original draft.

Tuoyu Zhou: Methodology, Validation.

Weilin Jin: Methodology, Resources.

Simin Zong: Investigation.

Tursunay Mamtimin: Investigation.

El-Sayed Salama: Resources.

Byong-Hun Jeon: Resources.

Pu Liu: Resources.

Huawen Han: Writing – review & editing, Supervision, Resources.

Xiangkai Li: Conceptualization & design; Project administration, Funding acquisition, Supervision.

Declaration of competing interest

The authors declare that they have no known competing financial interests or personal relationships that could have appeared to influence the work reported in this paper.

Data availability

The raw sequencing reads from 16S rRNA gene sequencing and metagenomic sequencing have been deposited separately in the NCBI Sequence Read Archive database (accession numbers: PRJNA907521 and PRJNA907967). Additional data supporting this study are available from the corresponding authors on reasonable request.

Acknowledgments

This work was supported by the National Natural Science Foundation of China (No. 32070117, 32200080), International Science and Technology Cooperation Project of Gansu Province (No. 2021-0204-GHC-0019) and Gansu Association for Science and Technology Innovation-Driven Boosting Project (No. GKX20210506-16-5). The authors appreciate the Central Lab of College of Life Science, Lanzhou University for providing instruments and equipment, as well as the Majorbio and Personalbio (Shanghai, China) for providing sequencing service. The authors also appreciate the contributions of Yanyi Chen, Wenxue Wang, Zemin Wang and Kunyue Zhang in sample collection.

Appendix A. Supplementary data

Supplementary data to this article can be found online at <https://doi.org/10.1016/j.lfs.2023.121709>.

References

- [1] H. Sung, J. Ferlay, R.L. Siegel, et al., Global cancer statistics 2020: GLOBOCAN estimates of incidence and mortality worldwide for 36 cancers in 185 countries, *CA Cancer J. Clin.* 71 (3) (2021) 209–249.
- [2] E. Dekker, P.J. Tanis, J.L.A. Vleugels, P.M. Kasi, M.B. Wallace, Colorectal cancer, *Lancet* 394 (10207) (2019) 1467–1480.
- [3] I. Marmol, C. Sanchez-de-Diego, A. Pradilla Dieste, E. Cerrada, M.J. Rodriguez Yoldi, Colorectal carcinoma: a general overview and future perspectives in colorectal cancer, *Int. J. Mol. Sci.* 18 (1) (2017) 197.
- [4] W.S. Garrett, The gut microbiota and colon cancer, *Science* 364 (6446) (2019) 1133–1135.
- [5] Y. Wu, N. Jiao, R. Zhu, et al., Identification of microbial markers across populations in early detection of colorectal cancer, *Nat. Commun.* 12 (1) (2021) 3063.
- [6] M. Rebersek, Gut microbiome and its role in colorectal cancer, *BMC Cancer.* 21 (1) (2021) 1325.
- [7] Y. Yang, W. Weng, J. Peng, et al., *Fusobacterium nucleatum* increases proliferation of colorectal cancer cells and tumor development in mice by activating toll-like receptor 4 signaling to nuclear factor- κ B, and up-regulating expression of MicroRNA-21, *Gastroenterology* 152 (4) (2017) 851–866.e824.
- [8] A. Iftikhar, H. Berger, N. Bouznad, et al., Genomic aberrations after short-term exposure to colibactin-producing *E. Coli* transform primary colon epithelial cells, *Nat. Commun.* 12 (1) (2021) 1003.
- [9] Q. Feng, S. Liang, H. Jia, et al., Gut microbiome development along the colorectal adenoma-carcinoma sequence, *Nat. Commun.* 6 (1) (2015) 6528.
- [10] S. Zhao, P. Feng, X. Hu, et al., Probiotic *limosilactobacillus fermentum* GR-3 ameliorates human hyperuricemia via degrading and promoting excretion of uric acid, *iScience* 25 (10) (2022), 105198.
- [11] W. Fong, Q. Li, J. Yu, Gut microbiota modulation: a novel strategy for prevention and treatment of colorectal cancer, *Oncogene* 39 (26) (2020) 4925–4943.
- [12] E.D. Kuugbee, X. Shang, Y. Gamallat, et al., Structural change in microbiota by a probiotic cocktail enhances the gut barrier and reduces cancer via TLR2 signaling in a rat model of colon cancer, *Dig. Dis. Sci.* 61 (10) (2016) 2908–2920.
- [13] L.E. Miller, L. Lehtoranta, M.J. Lehtinen, The effect of *bifidobacterium animalis* ssp. *Lactis* HN019 on cellular immune function in healthy elderly subjects: systematic review and meta-analysis, *Nutrients* 9 (3) (2017) 191.
- [14] B.F. Sieow, K.S. Wun, W.P. Yong, I.Y. Hwang, M.W. Chang, Tweak to treat: reprogramming bacteria for cancer treatment, *Trends Cancer.* 7 (5) (2021) 447–464.
- [15] L. Wu, F. Bao, L. Li, X. Yin, Z. Hua, Bacterially mediated drug delivery and therapeutics: strategies and advancements, *Adv. Drug Deliv. Rev.* 187 (2022), 114363.
- [16] J. Ma, Y. Lyu, X. Liu, et al., Engineered probiotics, *Microb. Cell Factories.* 21 (1) (2022) 72.
- [17] C.L. Ho, H.Q. Tan, K.J. Chua, et al., Engineered commensal microbes for diet-mediated colorectal-cancer chemoprevention, *Nat. Biomed. Eng.* 2 (1) (2018) 27–37.
- [18] V. Punj, S. Bhattacharyya, D. Saint-Dic, et al., Bacterial cupredoxin azurin as an inducer of apoptosis and regression in human breast cancer, *Oncogene* 23 (13) (2004) 2367–2378.
- [19] N. Mehta, J.G. Lyon, K. Patil, N. Mokarram, C. Kim, R.V. Bellamkonda, Bacterial carriers for glioblastoma therapy, *Mol. Ther. Oncolytics.* 4 (2017) 1–17.

- [20] M.A. Warso, J.M. Richards, D. Mehta, et al., A first-in-class, first-in-human, phase I trial of p28, a non-HDM2-mediated peptide inhibitor of p53 ubiquitination in patients with advanced solid tumours, *Br. J. Cancer*. 108 (5) (2013) 1061–1070.
- [21] A. Boleij, R.M. Schaepe, S. de Kleijn, et al., Surface-exposed histone-like protein a modulates adherence of streptococcus gallolyticus to colon adenocarcinoma cells, *Infect. Immun.* 77 (12) (2009) 5519–5527.
- [22] A. Yaghoubi, M. Khazaei, A. Avan, S.M. Hasanian, W.C. Cho, S. Soleimanpour, p28 bacterial peptide, as an anticancer agent, *Front. Oncol.* 10 (2020) 1303.
- [23] Y. Zhang, Y. Zhang, L. Xia, et al., Escherichia coli nissle 1917 targets and restrains mouse B16 melanoma and 4T1 breast tumors through expression of azurin protein, *Appl. Environ. Microbiol.* 78 (21) (2012) 7603–7610.
- [24] H.C. Jung, J.M. Lebeault, J.G. Pan, Surface display of zymomonas mobilis levansucrase by using the ice-nucleation protein of pseudomonas syringae, *Nat. Biotechnol.* 16 (6) (1998) 576–580.
- [25] K. Kim, J.H. Jeong, D. Lim, et al., L-asparaginase delivered by salmonella typhimurium suppresses solid tumors, *Mol. Ther. Oncolytics*. 2 (2015) 15007.
- [26] Y. Gong, Y. Wu, A. Khan, et al., Improving selenium accumulation in broilers using Escherichia coli nissle 1917 with surface-displayed selenite reductase SerV01, *Food Funct.* 13 (8) (2022) 4537–4550.
- [27] J. Boudeau, A.L. Glasser, S. Julien, J.F. Colombel, A. Darfeuille-Michaud, Inhibitory effect of probiotic Escherichia coli strain nissle 1917 on adhesion to and invasion of intestinal epithelial cells by adherent-invasive E. Coli strains isolated from patients with Crohn's disease, *Aliment. Pharmacol. Ther.* 18 (1) (2003) 45–56.
- [28] B. Jiang, L. Tian, X. Huang, et al., Characterization and antitumor activity of novel exopolysaccharide APS of lactobacillus plantarum WLPL09 from human breast milk, *Int. J. Biol. Macromol.* 163 (2020) 985–995.
- [29] M. Liu, P. Feng, A. Kakade, et al., Reducing residual antibiotic levels in animal feces using intestinal Escherichia coli with surface-displayed erythromycin esterase, *J. Hazard. Mater.* 388 (2020), 122032.
- [30] J. Feng, M. Lu, J. Wang, et al., Dietary oregano essential oil supplementation improves intestinal functions and alters gut microbiota in late-phase laying hens, *J. Anim. Sci. Biotechnol.* 12 (1) (2021) 72.
- [31] S. Chen, Y. Zhou, Y. Chen, J. Gu, Fastp: an ultra-fast all-in-one FASTQ preprocessor, *Bioinformatics* 34 (17) (2018) i884–i890.
- [32] H. Li, R. Durbin, Fast and accurate short read alignment with burrows-wheeler transform, *Bioinformatics* 25 (14) (2009) 1754–1760.
- [33] D. Li, C.-M. Liu, R. Luo, K. Sadakane, T.-W. Lam, MEGAHIT: an ultra-fast single-node solution for large and complex metagenomics assembly via succinct de bruijn graph, *Bioinformatics* 31 (10) (2015) 1674–1676.
- [34] H. Noguchi, J. Park, T. Takagi, MetaGene: prokaryotic gene finding from environmental genome shotgun sequences, *Nucleic Acids Res.* 34 (19) (2006) 5623–5630.
- [35] L. Fu, B. Niu, Z. Zhu, S. Wu, W. Li, CD-HIT: accelerated for clustering the next-generation sequencing data, *Bioinformatics* 28 (23) (2012) 3150–3152.
- [36] R. Li, Y. Li, K. Kristiansen, J. Wang, SOAP: short oligonucleotide alignment program, *Bioinformatics* 24 (5) (2008) 713–714.
- [37] B. Buchfink, C. Xie, D.H. Huson, Fast and sensitive protein alignment using DIAMOND, *Nat. Methods*. 12 (1) (2015) 59–60.
- [38] C. Piñero-Lambea, G. Bodelón, R. Fernández-Periáñez, A.M. Cuesta, L. Álvarez-Vallina, L. Fernández, Programming controlled adhesion of E. Coli to target surfaces, cells, and tumors with synthetic adhesins, *ACS Synth. Biol.* 4 (4) (2015) 463–473.
- [39] M. Bereta, A. Hayhurst, M. Gajda, et al., Improving tumor targeting and therapeutic potential of salmonella VNP20009 by displaying cell surface CEA-specific antibodies, *Vaccine* 25 (21) (2007) 4183–4192.
- [40] T.V. Plavec, A. Mitrovic, M. Perisic Nanut, B. Strukelj, J. Kos, A. Berlec, Targeting of fluorescent lactococcus lactis to colorectal cancer cells through surface display of tumour-antigen binding proteins, *Microb. Biotechnol.* 14 (5) (2021) 2227–2240.
- [41] B. Cheng, M. Montmasson, L. Terradot, P. Rousselle, Syndecans as cell surface receptors in cancer biology. A focus on their interaction with PDZ domain proteins, *Front. Pharmacol.* 7 (2016) 10.
- [42] S.D. Rosen, H. Lemjabbar-Alaoui, Sulf-2: an extracellular modulator of cell signaling and a cancer target candidate, *Expert Opin. Ther. Targets*. 14 (9) (2010) 935–949.
- [43] B.N. Taylor, R.R. Mehta, T. Yamada, et al., Noncationic peptides obtained from azurin preferentially enter cancer cells, *Cancer Res.* 69 (2) (2009) 537–546.
- [44] Z. Ye, H. Peng, Y. Fang, J. Feng, D.S. Yang, The construction of the eukaryotic expression plasmid pcDNA3.1/azurin and the increased apoptosis of U2OS cells transfected with it, *Cell. Mol. Biol. Lett.* 12 (3) (2007) 407–421.
- [45] M.L. Clapper, H.S. Cooper, W.-C.L. Chang, Dextran sulfate sodium-induced colitis-associated neoplasia: a promising model for the development of chemopreventive interventions, *Acta Pharmacol. Sin.* 28 (9) (2007) 1450–1459.
- [46] M.A. Marie, E.J. Sanderlin, S. Satturwar, et al., GPR65 (TDAG8) inhibits intestinal inflammation and colitis-associated colorectal cancer development in experimental mouse models, *Biochim. Biophys. Acta Mol. basis Dis.* 1868 (1) (2022), 166288.
- [47] N. Hattori, T. Niwa, T. Ishida, et al., Antibiotics suppress colon tumorigenesis through inhibition of aberrant DNA methylation in an azoxymethane and dextran sulfate sodium colitis model, *Cancer Sci.* 110 (1) (2019) 147–156.
- [48] A.T. Sougiannis, B.N. VanderVeen, R.T. Enos, et al., Impact of 5 fluorouracil chemotherapy on gut inflammation, functional parameters, and gut microbiota, *Brain Behav. Immun.* 80 (2019) 44–55.
- [49] Y. Vodenkova, T. Buchler, K. Cervena, V. Veskrnova, P. Vodicka, V. Vymetalkova, 5-fluorouracil and other fluoropyrimidines in colorectal cancer: past, present and future, *Pharmacol. Ther.* 206 (2020), 107447.
- [50] Y. Chung, Y. Ryu, B.C. An, et al., A synthetic probiotic engineered for colorectal cancer therapy modulates gut microbiota, *Microbiome* 9 (1) (2021) 122.
- [51] J.M. Tucker, C. Davis, M.E. Kitchens, et al., Response to 5-fluorouracil chemotherapy is modified by dietary folic acid deficiency in ApcMin/+ mice, *Cancer Lett.* 187 (1) (2002) 153–162.
- [52] M. Guo, Z. Li, Polysaccharides isolated from Nostoc commune vaucher inhibit colitis-associated colon tumorigenesis in mice and modulate gut microbiota, *Food Funct.* 10 (10) (2019) 6873–6881.
- [53] J.M. Adams, S. Cory, The Bcl-2 apoptotic switch in cancer development and therapy, *Oncogene* 26 (9) (2007) 1324–1337.
- [54] G. Song, Y. Lu, Z. Yu, et al., The inhibitory effect of polysaccharide from rhizopus nigricans on colitis-associated colorectal cancer, *Biomed. Pharmacother.* 112 (2019), 108593.
- [55] N.S. Oh, J.Y. Lee, Y.T. Kim, S.H. Kim, J.H. Lee, Cancer-protective effect of a synbiotic combination between lactobacillus gasseri 505 and a Cudrania tricuspidata leaf extract on colitis-associated colorectal cancer, *Gut Microbes*. 12 (1) (2020), 1785803.
- [56] A. Ibrahim, L.W.S. Hugerth, L. Hases, et al., Colitis-induced colorectal cancer and intestinal epithelial estrogen receptor beta impact gut microbiota diversity, *Int. J. Cancer*. 144 (12) (2019) 3086–3098.
- [57] C. Guo, D. Guo, L. Fang, et al., Ganoderma lucidum polysaccharide modulates gut microbiota and immune cell function to inhibit inflammation and tumorigenesis in colon, *Carbohydr. Polym.* 267 (2021), 118231.
- [58] S.R. Konstantinov, E.J. Kuipers, M.P. Peppelenbosch, Functional genomic analyses of the gut microbiota for CRC screening, *Nat. Rev. Gastroenterol. Hepatol.* 10 (12) (2013) 741–745.
- [59] M. Molska, J. Regula, Potential mechanisms of probiotics action in the prevention and treatment of colorectal cancer, *Nutrients* 11 (10) (2019) 2453.
- [60] X. Liu, B. Mao, J. Gu, et al., Blautia—a new functional genus with potential probiotic properties? *Gut Microbes*. 13 (1) (2021), 1875796.
- [61] A. Nowak, A. Paliwoda, J. Biasiak, Anti-proliferative, pro-apoptotic and anti-oxidative activity of lactobacillus and bifidobacterium strains: a review of mechanisms and therapeutic perspectives, *Crit. Rev. Food Sci. Nutr.* 59 (21) (2019) 3456–3467.
- [62] M. Esлами, B. Yousefi, P. Kokhaei, et al., Importance of probiotics in the prevention and treatment of colorectal cancer, *J. Cell. Physiol.* 234 (10) (2019) 17127–17143.
- [63] R.Y. Hsu, C.H. Chan, J.D. Spicer, et al., LPS-induced TLR4 signaling in human colorectal cancer cells increases beta1 integrin-mediated cell adhesion and liver metastasis, *Cancer Res.* 71 (5) (2011) 1989–1998.
- [64] N. Gasaly, P. de Vos, M.A. Hermoso, Impact of bacterial metabolites on gut barrier function and host immunity: a focus on bacterial metabolism and its relevance for intestinal inflammation, *Front. Immunol.* 12 (2021), 658354.
- [65] Y. Fang, C. Yan, Q. Zhao, et al., The roles of microbial products in the development of colorectal cancer: a review, *Bioengineered* 12 (1) (2021) 720–735.
- [66] X. Li, Q. Chu, Y. Huang, et al., Consortium of probiotics attenuates colonization of clostridioides difficile, *Front. Microbiol.* 10 (2019) 2871.
- [67] L. Zhang, G. Tian, L. Huang, et al., Pterostilbene attenuates intestinal epithelial barrier loss induced by high loading intensity of exercise, *Front. Nutr.* 9 (2022), 965180.
- [68] Y.-H. Xie, Y.-X. Chen, J.-Y. Fang, Comprehensive review of targeted therapy for colorectal cancer, *Signal Transduct. Target. Ther.* 5 (1) (2020) 22.
- [69] F. Goirand, F. Lemaitre, M. Launay, et al., How can we best monitor 5-FU administration to maximize benefit to risk ratio? *Expert Opin. Drug Metab. Toxicol.* 14 (12) (2018) 1303–1313.
- [70] E. Van Cutsem, A. Cervantes, B. Nordlinger, D. Arnold, Metastatic colorectal cancer: ESMO clinical practice guidelines for diagnosis, treatment and follow-up, *Ann. Oncol.* 25 (2014) iii1–iii9.
- [71] M. Saeed, A. Shoaib, R. Kandimalla, et al., Microbe-based therapies for colorectal cancer: advantages and limitations, *Semin. Cancer Biol.* 86 (2022) 652–665.
- [72] R. Villéger, A. Lopès, G. Carrier, et al., Intestinal microbiota: a novel target to improve anti-tumor treatment? *Int. J. Mol. Sci.* 20 (18) (2019).
- [73] A. Badgeley, H. Anwar, K. Modi, P. Murphy, A. Lakshmiikuttyamma, Effect of probiotics and gut microbiota on anti-cancer drugs: mechanistic perspectives, *Biochim. Biophys. Acta Rev. Cancer*. 1875 (1) (2021), 188494.
- [74] E.M.M. Quigley, Probiotics and probiotics in digestive health, *Clin. Gastroenterol. Hepatol.* 17 (2) (2019) 333–344.
- [75] T. Ozdemir, A.J.H. Fedorec, T. Danino, C.P. Barnes, Synthetic biology and engineered live biotherapeutics: toward increasing system complexity, *Cell Syst.* 7 (1) (2018) 5–16.